PERGAMON

International Journal of Heat and Mass Transfer 42 (1999) 1363–1369

International Journal of HEAT and MASS TRANSFER

Heat transfer in micro region of a rotating miniature heat pipe

Lanchao Lin, Amir Faghri*

Department of Mechanical Engineering, University of Connecticut, Storrs, CT 06269-3139, U.S.A.

Received 12 September 1997; in final form 12 August 1998

Abstract

A theoretical model is established that describes the evaporating film flow in a rotating miniature heat pipe with an axial triangular grooved internal surface. The theory of thin liquid film vaporization heat transfer is used to predict the evaporation heat transfer in the micro region. The effects of disjoining pressure, surface tension and centrifugal force on the flow are discussed. Results show that the influence of centrifugal force on the liquid film flow and evaporation heat transfer in the micro region is not significant. The influence of superheat on the apparent contact angle and evaporation heat transfer coefficient in the micro region is shown.

Nomenclature

a coefficient [kg m^{-2} s^{-1} K^{-1}]
A dispersion constant [J]
b coefficient [s m^{-1}]
B parameter [N m^{-3}]
c_1 parameter
g gravitational acceleration [m s^{-2}]
h_{mic} evaporation heat transfer coefficient in micro region [W m^{-2} K^{-1}]
h_{fg} latent heat of evaporation [J kg^{-1}]
k conductivity [W m^{-1} K^{-1}]
K curvature [m^{-1}]
L_l length of groove liquid on the wall [m]
$\dot{m}'$ mass rate per unit axial length [kg m^{-1} s^{-1}]
M molecular weight [kg kmol^{-1}]
N rotational speed [rpm]
p pressure [N m^{-2}]
p_d disjoining pressure [N m^{-2}]
p_i pressure difference across the liquid–vapor interface [N m^{-2}]
q_{mic} heat flux in micro region [W m^{-2}]
Q'_l heat flow rate per unit groove length ($0 \leqslant x \leqslant 2\times10^{-7}$ m) [W m^{-1}]
r_{mic} distance from the heat pipe center line to micro region [m]
R_m radius of curvature of the meniscus [m]
R_u universal gas constant [J kmol^{-1} K^{-1}]
s_t radius [m]
T temperature [K]
u_l liquid velocity in the x-direction [m s^{-1}]
V_l molar volume of liquid [m^3 kmol^{-1}]
x coordinates [m]
y coordinates [m].

Greek symbols

α angle
γ half-angle of the groove
δ liquid film thickness [m]
ΔT temperature drop, $T_w - T_v$ [K]
η angle
θ apparent contact angle
μ dynamic viscosity [N s m^{-2}]
ρ mass density [kg m^{-3}]
σ surface tension [N m^{-1}]
τ_l liquid shear stress [N m^{-2}]
ω angular velocity [rad s^{-1}].

Subscripts

l liquid
mic micro region
v vapor
w wall
0 original point
δ liquid film free surface.

* Corresponding author. Tel.: 001 860 486 2221; fax: 001 860 486 0318; e-mail: faghri@eng2.uconn.edu

0017–9310/98/$ - see front matter
PII: S0017–9310(98)00270–1

1. Introduction

Rotating heat pipes have been successfully used in cooling electric motors and generators and could be used in drill bit cooling [1]. Many rotating heat pipe investigations have been accomplished concerning the internal heat transfer and hydrodynamic performance with internal diameters greater than 10 mm [2, 3]. Studies of rotating miniature heat pipes (RMHP), diameters less than 10 mm, have recently started and some results regarding steady-state performance and maximum heat transfer capacity have been reported [4].

A typical horizontally oriented rotating miniature heat pipe is shown in Fig. 1. The fluid flow in the rotating miniature heat pipe is characterized by axial fluid flows and liquid film flows transverse to the axial direction. Axial fluid flows include an axial liquid flow in the groove and a countercurrent vapor flow with varied mass rate due to evaporation and condensation. Liquid film flows transverse to the axial direction occur both in the evaporator and in the condenser. In the evaporator, an evaporating thin liquid film flow up the groove side wall is driven by the disjoining pressure and the surface tension. In the condenser, a condensate film flow into the groove is sustained by centrifugal force.

Kamotani [5] calculated the evaporation heat transfer through the micro region and the apparent contact angle. Holm and Goplen [6] conducted a one-dimensional analysis of the evaporation heat transfer through grooved wall surfaces. Stephan and Busse [7] developed a model which combined the thin liquid film vaporization heat transfer with the two-dimensional solution of the conduction heat transfer through the heat pipe wall and the liquid in the groove. It was concluded that the assumption of an interface temperature equal to the saturation temperature of the vapor can lead to a large overprediction of the radial heat transfer coefficient. Khrustalev and Faghri [8] developed a model describing heat transfer through thin liquid films in a heat pipe evaporator with capillary grooves. The model accounted for the effects of interfacial thermal resistance, disjoining pressure, and surface roughness for a given meniscus contact angle. The importance of the surface roughness in predicting the heat transfer coefficient in the grooved evaporator was demonstrated. Ma and Peterson [9] developed a model for the evaporation heat transfer coefficient and temperature variation along the axial direction of a grooved plate. The results obtained from this model indicated that if a constant heat flux boundary condition was applied, the heat transfer coefficient decreased and the wall temperature increased along the axial direction. In addition, the apparent contact angle was determined along the axial direction.

The mathematical model of the hydrodynamic performance of RMHPs has been developed [4]. Using the model, the maximum performance and optimum fill amount of RMHP have been predicted under various operating conditions. Evaporation heat transfer characteristics of RMHP have not been reported in the past. Basic theoretical investigations of conventional rotating heat pipes presented by Faghri [3] are helpful in establishing a model of liquid film flow on the groove side wall in RMHP. In the condenser, the centrifugal force field is not constant regarding the condensate film flow on the groove side wall, while in the evaporator it can be regarded as constant in the micro region. Theory of thin liquid film vaporization heat transfer, summarized by Faghri [3] is used in the analysis of the RMHP evaporation heat transfer.

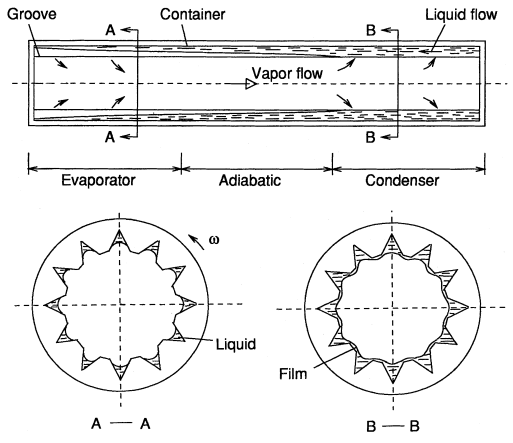

Fig. 1. Performance of an axially rotating miniature heat pipe (RMHP) with a polygonal inner wall with axial triangular grooves.

2. Modeling

As shown in Fig. 1, an axially rotating miniature heat pipe is horizontally oriented. It is comprised of a series of axial triangular grooves machined along the inner wall to provide condensate return paths or liquid channels. Vaporization and condensation causes the liquid–vapor interface geometry in the liquid channels to change continuously along the axial length. A change in radius of curvature of the liquid–vapor interface causes a capillary pressure difference between the condenser and evaporator, which promotes the flow of condensate back to the evaporator. In addition, a varying liquid depth allows the centrifugal acceleration to produce a hydrostatic pressure change along the groove which pumps the condensate back to the evaporator. Counter-flowing vapor exerts a shear force at the liquid free surface. To obtain a high internal heat transfer coefficient and to prevent flooding of the countercurrent flow during operation of the RMHP, the liquid fill is controlled to ensure that no

excess liquid blocks the condenser. The change in radius of curvature of the liquid–vapor interface along the axial direction can be predicted through the analysis of axial fluid flows [4].

In the present analysis of the heat transfer in the micro region, the radius of curvature of the liquid–vapor interface in the meniscus region as shown in Fig. 2 is constant. In the evaporator, the polygonal wall surface is dry as shown in Fig. 2. On the groove side wall of the evaporator, the extended meniscus is typically divided into three regions such as the meniscus region, evaporating thin film region and non evaporating region (adsorbed layer region). The flow in the evaporating thin film region is governed by the disjoining pressure and surface tension. The adsorbed layer where no vaporization occurs is dominated by the disjoining pressure.

The coordinate system for the evaporating thin film flow is shown in Fig. 2. The assumptions made are as follows: The vapor temperature, T_v, and the wall temperature, T_w, are constant; the radius of curvature of the liquid–vapor interface in the meniscus region and the rotational radius of the micro region, r_{mic}, are constant; the influences of the Coriolis force, gravitational force and vapor drag on the evaporating thin film flow are negligible. A static force balance in the x and y directions on a differential element in the evaporating thin film on the groove side wall, as shown in Fig. 2, gives the following:

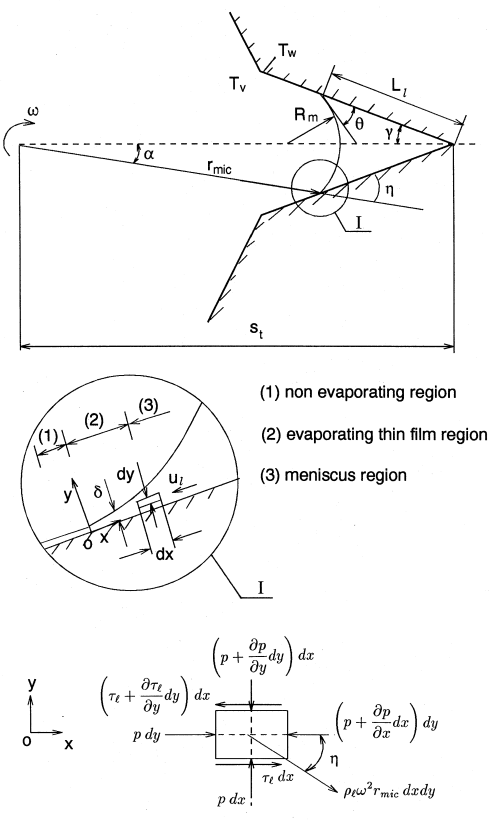

Fig. 2. Force balance in a differential control volume of the evaporating thin film and coordinate system.

$$\frac{\partial p_l}{\partial y} + \rho_l \omega^2 r_{mic} \sin\eta = 0 \tag{1}$$

$$-\frac{\partial p_l}{\partial x} + \rho_l \omega^2 r_{mic} \cos\eta - \frac{\partial \tau_l}{\partial y} = 0. \tag{2}$$

where η is the angle between the x coordinate and extended line of r_{mic} and τ_l is the liquid shear stress which is expressed as

$$\tau_l = \mu_l \frac{\partial u_l}{\partial y}. \tag{3}$$

The following geometrical relations can be established.

$$L_l = \frac{R_m \cos(\gamma+\theta)}{\sin\gamma} \tag{4}$$

$$\cos\alpha = \frac{s_t - L_l \cos\gamma}{r_{mic}} \tag{5}$$

$$\sin\alpha = \frac{L_l \sin\gamma}{r_{mic}} \tag{6}$$

$$r_{mic}\cos\eta = r_{mic}\cos(\gamma+\alpha) = s_t\cos\gamma - L_l \tag{7}$$

$$r_{mic}\sin\eta = r_{mic}\sin(\gamma+\alpha) = s_t\sin\gamma. \tag{8}$$

Using eqns (7), (8) and (3), eqns (1) and (2) become

$$\frac{\partial p_l}{\partial y} + \rho_l \omega^2 s_t \sin\gamma = 0 \tag{9}$$

$$-\frac{\partial p_l}{\partial x} + \rho_l \omega^2 (s_t\cos\gamma - L_l) - \mu_l \frac{\partial^2 u_l}{\partial y^2} = 0. \tag{10}$$

A boundary condition at the liquid–vapor interface is related to the following relation of the pressure difference across the liquid–vapor interface:

$$p_i = p_v - p_l = \sigma K + p_d \quad \text{at} \quad y = \delta \tag{11}$$

The first term on the right-hand side of eqn (11) describes the surface tension effect, and the curvature of the interface, K, can be determined by

$$K = \frac{d^2\delta}{dx^2}\left[1+\left(\frac{d\delta}{dx}\right)\right]^{-3/2}. \tag{12}$$

The second term expresses the disjoining pressure. For nonpolar liquids $p_d = A/\delta^3$ [10] where A is the dispersion constant. Combined with eqn (11), eqn (12) can be written in another form:

$$\frac{d\delta}{dx} = t \tag{13}$$

$$\frac{dt}{dx} = \frac{1}{\sigma}\left(p_i - \frac{A}{\delta^3}\right)(1+t^2)^{3/2} \tag{14}$$

In addition to the above condition, the negligence of vapor drag on the film surface states

$$\frac{\partial u_l}{\partial y} = 0 \quad \text{at} \quad y = \delta. \tag{15}$$

The no-slip condition at the groove side wall is

$$u_l = 0 \quad \text{at} \quad y = 0. \tag{16}$$

Integrating the static force balance in the y direction, eqn (9), yields

$$p_l = \rho_l \omega^2 s_t \sin\gamma(\delta - y) - p_i + p_v. \tag{17}$$

Differentiating eqn (17) with respect to x yields

$$\frac{dp_l}{dx} = \rho_l \omega^2 s_t \sin\gamma \frac{d\delta}{dx} - \frac{dp_i}{dx}. \tag{18}$$

Introducing

$$B = -\frac{dp_i}{dx} + \rho_l \omega^2 s_t \sin\gamma \frac{d\delta}{dx} - \rho_l \omega^2 (s_t \cos\gamma - L_l), \tag{19}$$

eqn (10) becomes

$$B = -\mu_l \frac{\partial^2 u_l}{\partial y^2}. \tag{20}$$

Solving eqn (20) gives

$$u_l = \frac{B}{\mu_l}\left(y - \frac{y^2}{2}\right). \tag{21}$$

The mass rate per unit axial length of the film is given by

$$\dot{m}' = \rho_l \int_0^\delta u_l \, dy = \frac{\rho_l B \delta^3}{3\mu_l}. \tag{22}$$

Substituting B from eqn (22) into eqn (19) gives

$$\frac{dp_i}{dx} = -\frac{3\mu_l \dot{m}'}{\rho_l \delta^3} - \rho_l \omega^2 (s_t \cos\gamma - L_l) + \rho_l \omega^2 s_t \sin\gamma \frac{d\delta}{dx}. \tag{23}$$

Assuming that

$$s_t \cos\gamma - L_l \gg s_t \sin\gamma \frac{d\delta}{dx}, \tag{24}$$

simplifies eqn (23) to

$$\frac{dp_i}{dx} = -\frac{3\mu_l \dot{m}'}{\rho_l \delta^3} - \rho_l \omega^2 (s_t \cos\gamma - L_l). \tag{25}$$

The mass rate per unit axial length of the film can be related to a kinetic model of the evaporating mass flux of vapor leaving the liquid–vapor interface. The following expression for evaporating mass flux, $d\dot{m}'/dx$, developed by Schonberg and Wayner [10] is used.

$$\frac{d\dot{m}'}{dx} = a(T_\delta - T_v) + b(p_l - p_v), \tag{26}$$

where

$$a = 2.0\left(\frac{M}{2\pi R_u T_\delta}\right)^{1/2}\left(\frac{p_v M h_{fg}}{R_u T_v T_\delta}\right), \tag{27}$$

$$b = 2.0\left(\frac{M}{2\pi R_u T_\delta}\right)^{1/2}\left(\frac{V_l p_v}{R_u T_\delta}\right). \tag{28}$$

The temperature of the liquid at the liquid–vapor interface is related to the temperature of the inner wall, T_w, through a one-dimensional heat conduction model:

$$\frac{d\dot{m}'}{dx} = \frac{k_l}{\delta h_{fg}}(T_w - T_\delta). \tag{29}$$

Combining eqn (26) and eqn (29) eliminates T_δ:

$$\frac{d\dot{m}'}{dx} = \left(1 + \frac{a\delta h_{fg}}{k_l}\right)^{-1}[a(T_w - T_v) - bp_i]. \tag{30}$$

The evaporating heat flux in the micro region, q_{mic}, is

$$q_{mic} = \frac{d\dot{m}'}{dx} h_{fg}. \tag{31}$$

The evaporation heat transfer coefficient in the micro region is defined as

$$h_{mic} = \frac{q_{mic}}{\Delta T}, \tag{32}$$

where $\Delta T = T_w - T_v$. At $x = 0$, the film thickness is so small that no evaporation occurs. This value is referred to as δ_0 and is obtained by setting the mass flux and the meniscus curvature equal to zero:

$$\delta_0 = \left(\frac{bA}{a\Delta T}\right)^{1/3}. \tag{33}$$

The pressure difference across the liquid vapor interface at $x = 0$ is

$$p_{i,0} = \frac{A}{\delta_0^3}. \tag{34}$$

Corresponding to eqns (13), (14), (25) and (30), the boundary conditions at $x = 0$ are

$$\delta = \delta_0 \tag{35}$$

$$\frac{d\delta}{dx} = 0 \tag{36}$$

$$p_i = p_{i,0} \tag{37}$$

$$\dot{m}' = 0. \tag{38}$$

In addition, the solution of the ordinary differential equations, i.e. (13), (14), (25) and (30), should satisfy one more condition that as the disjoining pressure, p_d, approaches a sufficiently small value, ε (e.g. $\varepsilon = 0.001 p_i$), p_i reaches a constant:

$$p_i|_{p_d = \varepsilon} = \frac{\sigma}{R_m}. \tag{39}$$

The corresponding location is denoted by x_m. The apparent contact angle (the angle between the solid–liquid and liquid–vapor interfaces), θ, at the location x_m is given by

$$\tan\theta = \left(\frac{d\delta}{dx}\right)_{x = x_m}. \tag{40}$$

3. Numerical treatment

The four ordinary differential equations (ODEs), (13), (14), (25) and (30) are solved using an ODEs integrator

LSODE [11]. LSODE solves ODEs using Newton's method in the corrector step. Given a set of boundary conditions, a profile of liquid–vapor interface can be obtained. However, the profile probably does not satisfy condition (39). Numerical experiments show that a minor change in boundary conditions (35) and (37) can result in a notable change in p_i as p_d approaches ε. Therefore, the ODEs solution procedure is as follows. Given a value of δ at $x = 0$, $\delta = \delta_0(1+c_1)$, where c_1 is smaller than 0.01, a shooting method on parameter $p_{i,0}$ is used to make the solution satisfy condition (39). At the same time, boundary conditions (36) and (38) are used. The integration is stopped at a location where the change of curvature, K, with the x coordinate becomes negligible. Numerical results for different values of c_1 are compared. It is indicated that if $c_1 < 0.01$, the relative difference of the predicted parameters, δ, $d\delta/dx$, p_i and $\dot{m}'$ for the different values of c_1 is less than $\pm 3\%$ in the evaporating thin film region. The slope of the predicted meniscus determines the apparent contact angle. The relative error involved in the integration is controlled to be less than 10^{-8} for each of the variables.

4. Results and discussion

Characteristics of the rotating miniature heat pipe used for evaporation heat transfer simulation are as follows: $s_t = 2.0$ mm, $\gamma = 20^\circ$ and $R_m = 0.14$ mm. Ammonia is chosen as the working fluid and the heat pipe wall material is copper. The operating temperature, T_v is 300 K. The dispersion constant is chosen to be 2×10^{-21} J [7].

Figure 3 shows comparison between the predicted results for $c_1 = 0.01$ and $c_1 = 0.005$. The heat flux distribution and film thickness distribution move slightly to the right-hand side for smaller c_1. In the region of $x > 0.2 \times 10^{-7}$ m, the relative differences of q_{mic} and δ for

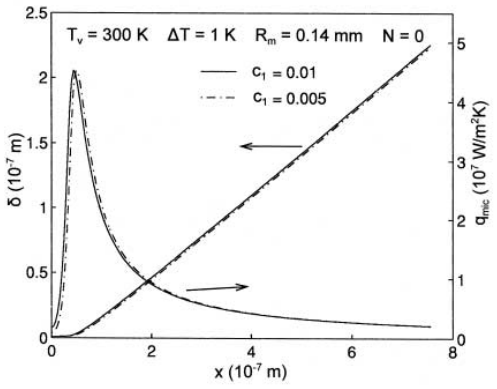

Fig. 3. Heat flux and film thickness as functions of the x coordinate in the micro region for two different parameters of c_1.

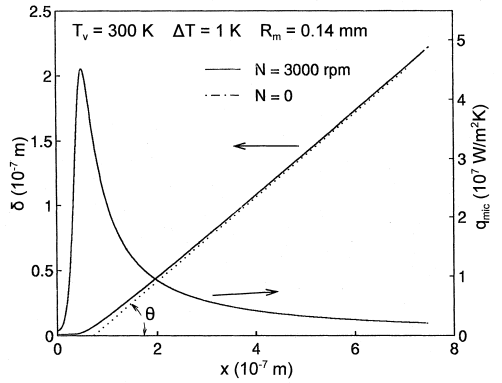

Fig. 4. Heat flux and film thickness as functions of the x coordinate in the micro region for the cases of $N = 0$ and $N = 3000$ rpm.

the different values of c_1 are less than 3%. Therefore, c_1 is chosen to be 0.005 in the following numerical simulation. The predicted results of q_{mic} and δ for $N = 3000$ rpm and $N = 0$ are presented in Fig. 4. The curves of q_{mic} and δ for $N = 3000$ rpm and those for $N = 0$ almost overlap in the micro region. It means that the influence of the rotational speed on the evaporation heat transfer in the micro region can be neglected. Therefore, the heat transfer analysis in the micro region at $N = 0$ can be applied to the case of rotational operation. The momentum equations, (1) and (2), for liquid film flow can also be used for the analysis of condensation heat transfer on the condenser groove side wall. It is expected that the centrifugal field will influence the condensation heat transfer through the condensate film. The evaporation heat flux is a very small value at the initial location. The evaporation heat flux increases dramatically up to the maximum value and then decreases with the x coordinate. As the film thickness increases along the x direction, the disjoining pressure tends to be negligibly small and the film meniscus approaches a nearly constant slope. The apparent contact angle is indicated by extending the slope of the δ curve at $x = x_m$ where condition (39) is satisfied.

Figure 5 shows the temperature difference and pressure difference across the liquid–vapor interface as functions of the x coordinate in the micro region. The value of p_i reaches its maximum at $x = 0$ and tends to decrease with the x coordinate close to the original point. As $x > 10^{-8}$ m, p_i drops rapidly and approaches an asymptotic value of σ/R_m. The decrease of $T_\delta - T_v$ with the evaporating thin film is moderate compared to the curve of p_i. The interfacial thermal resistance is still significant even when the film thickness is larger than 1×10^{-7} m. The superheat effect on liquid film thickness distribution in the micro region is shown in Fig. 6. The film thickness and apparent contact angle increase with an increase of superheat. Figure 7 shows the superheat effect on the distribution of

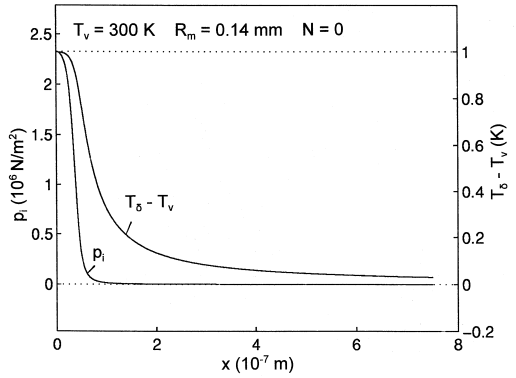

Fig. 5. Temperature difference and pressure difference across the liquid–vapor interface as functions of the x coordinate in the micro region.

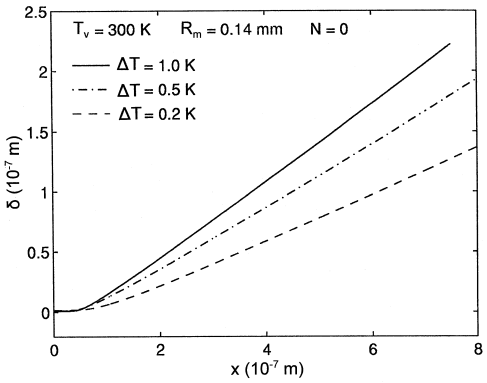

Fig. 6. Superheat effect on liquid film thickness distribution in the micro region.

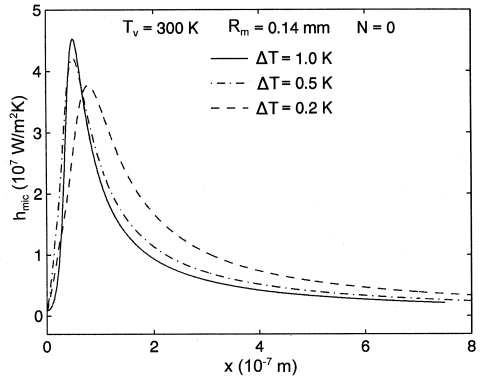

Fig. 7. Superheat effect on the distribution of evaporation heat transfer coefficient in the micro region.

Table 1
Comparison of present predictions with reported results

Parameters	Stephan and Busse [7]	Present predictions	
		$c_1 = 0.01$	$c_1 = 0.005$
R_m (mm)		0.14	0.14
$T_w - T_v$ (K)	1.0	1.0	1.0
$q_{mic,m}$ (W m^{-2})	5.3×10^7	4.52×10^7	4.52×10^7
Q'_1 (W m^{-1}) $(0 \leqslant x \leqslant 2 \times 10^{-7}$ m)	3.4	3.96	3.91
θ (°)	19.7	18.11	18.10

evaporation heat transfer coefficient, h_{mic}, along the evaporating thin film. As the superheat increases, the curve of h_{mic} becomes sharper and the maximum value of the curve increases. On the right-hand part where h_{mic} decreases with the x coordinate, higher superheat results in a lower h_{mic}.

A comparison with the numerical data reported by Stephan and Busse [7] has been made. The properties of working fluid, the wall material and dispersion constant used in the present analysis are the same as those used by them. Comparison items and calculation results are listed in Table 1 where $q_{mic,m}$ is the maximum heat flux in the micro region and Q'_1 is the heat flow rate per unit groove length in the region of $0 \leqslant x \leqslant 2 \times 10^{-7}$ m. Q'_1 is calculated by $Q'_1 = h_{fg}\dot{m}'$ at $x = 2 \times 10^{-7}$ m. The present predictions are given for $c_1 = 0.01$ and $c_1 = 0.005$ respectively. The corresponding results for the different values of c_1 are very close. The value of $q_{mic,m}$ presented by Stephan and Busse [7] is about 17% larger than the present result, while the value of Q'_1 is about 13% smaller than the present result. The comparison is satisfactory.

5. Conclusions

Evaporation heat transfer characteristics in the micro region of a rotating miniature heat pipe is numerically simulated based on the present mathematical model and the results are summarized as follows:

1. The influence of the rotational speed on the evaporation heat transfer in the micro region can be neglected. Therefore, the heat transfer analysis in the micro region at $N = 0$ can be applied to the case of rotational operation.
2. It is indicated that as the film thickness increases along the x direction, the disjoining pressure tends to be negligibly small and the film meniscus approaches a nearly constant slope.
3. The film thickness and apparent contact angle increase with an increase of superheat.

4. The comparison of the present results with the reported numerical data is satisfactory.

References

[1] V.H. Gray, Method and apparatus for heat transfer in rotating bodies, U.S. Patent No. 3 842 596 (1974).

[2] P.J. Marto, Rotating heat pipes. XIV, ICHTM Symposium 'Heat and Mass Transfer in Rotating Machinery' Dubrovnik, 1982.

[3] A. Faghri, Heat Pipe Science and Technology. Taylor & Francis, Washington, DC, 1995.

[4] L. Lin, A. Faghri, Steady-state performance of a rotating miniature heat pipe, J. Thermophysics and Heat Transfer 11 (4) (1997) 513–518.

[5] Y. Kamotani, Evaporator film coefficients of grooved heat pipes, Proceedings of the 3rd International Heat Pipe Conference, Palo Alto, CA, 1978.

[6] F.W. Holm, S.P. Goplen, Heat transfer in the thin-film region, J. Heat Transfer 101 (1979) 543–547.

[7] P.C. Stephan, C.A. Busse, Analysis of the heat transfer coefficient of grooved heat pipe evaporator walls, Int. J. Heat Mass Transfer 35 (2) (1992) 383–391.

[8] D. Khrustalev, A. Faghri, Heat transfer during evaporation on capillary-grooved structures of heat pipes, J. Heat Transfer 117 (3) (1995) 740–747.

[9] H.B. Ma, G.P. Peterson, Temperature variation and heat transfer in triangular grooves with an evaporating film, J. Thermophysics and Heat Transfer 11 (1) (1997) 90–97.

[10] J. Schonberg, P. Wayner, An analytical solution for the integral contact line evaporative heat sink, J. Thermophysics and Heat Transfer 6 (1) (1992) 128–134.

[11] A.C. Hindmarsh, ODEPACK, a systematized collection of ODE solvers, in: Scientific Computing, R.S. Stepleman (Ed.), North-Holland, Amsterdam, 1983 pp. 55–64.